Proceedings of the the Tenth Symposium of Magnetic Measurements, Warsaw, 17–19.10.2011

Structural and Magnetic Features of $Mn_{1-x}Zn_xFe_2O_4$ Nanoparticles

A. Mendoza[a], J. Prado[b], O. Almanza[c]

[a] Magnetic Materials and Nanostructures Group, Phys. Dep., Universidad Nacional de Colombia Carrera 45 No 26–85, Bogotá, Colombia

[b] Excellence Center for Novel Materials, CENM, Calle 13 N.100–00 Building 320 ofice 1030, Cali, Colombia,

[c] Physics Department, Universidad Nacional de Colombia, Carrera 45 No 26–85, Bogotá, Colombia

This paper reports on the magnetic properties of $Mn_{1-x}Zn_x$-ferrite nanoparticles. Different x compositions of the magnetic material have been considered. Field- and temperature-dependent magnetization curves and electron paramagnetic resonance (EPR) at different temperatures were used to reveal the magnetic properties of the samples. For $x = 0.5$, the EPR spectra consist of a single resonance signal, strongly symmetrical, with $g = 3.25$ close to 2073 G, and an asymmetric line corresponding to $g = 4.4$ for $x = 0$. The asymmetry is attributed to a random distribution of the anisotropy in the system, with perpendicular and parallel modes, giving information about the effective anisotropy of the system. For high concentrations, the resonant field shifts to 2875 G. Magnetization measurements as function of temperature at 60 Oe according to the standard zero field cooling (ZFC) and field cooling (FC) procedures are reported. The behavior of field cooling magnetization (MFC) at low temperatures evidences the presence of strong interparticles interactions.

PACS: 75.75.Fk, 75.30.Gw, 75.60.Ch, 75.50.Gg

1. Introduction

One of the most active areas of materials research is the behavior of nanostructured media. Nanocrystalline spinel ferrites find important applications in many engineering areas. They are used, for example, in miniaturization of electronic devices. Moreover, nanoparticle ferrites are considered outstanding materials for high-density magnetic recording, since their magnetic properties differ markedly from single ferrites [1]. Other practical areas of importance are medical diagnosis and biomedical applications [2, 3]. $Mn_xZn_{1-x}Fe_2O_4$ belongs to the group of cubic spinel structures with magnetic ions Fe^{3+}, and Fe^{2+} distributed in octahedral and tetrahedral sites, depending on the x-value (see Table I) [4].

TABLE I

Cation distribution for $Mn_{1-x}Zn_xFe_2O_4$. Square and round brackets for octahedral sites (3+) and tetrahedral sites (2+) respectively. Fe represents the iron ions with reversed spins

Ionic Formula [4]
$(Mn_{0.84}Fe_{0.16})$ $[Fe_{1.84}Mn_{0.16}]$ O_4
$(Zn_{0.20}Mn_{0.68}Fe_{0.12})$ $[\underline{Fe}_{1.88}Mn_{0.12}]$ O_4
$(Zn_{0.40}Mn_{0.53}Fe_{0.07})$ $[\underline{Fe}_{1.93}Mn_{0.07}]$ O_4
$(Zn_{0.60}Mn_{0.40})$ $[\underline{Fe}_{0.17}Fe_{1.83}]$ O_4
$(Zn_{0.70}Mn_{0.30})$ $[\underline{Fe}_{0.33}Fe_{1.67}]$ O_4
$(Zn_{0.80}Mn_{0.20})$ $[\underline{Fe}_{0.46}Fe_{1.54}]$ O_4
$(Zn_{0.90}Mn_{0.10})$ $[\underline{Fe}_{0.68}Fe_{1.35}]$ O_4
$(Zn_{0.95}Mn_{0.05})$ $[\underline{Fe}_{0.46}Mn_{1.54}]$ O_4

The magnetic properties of the ferrite nanoparticles are found to undergo changes because of superparamagnetism, surface spin effects, and cation distribution, which depends mainly on the stoichiometry and synthesis method [5, 6]. Among the many experimental research methods to study the magnetic properties of the ferrite nanoparticles, electron paramagnetic resonance (EPR) proves to be a useful and sensitive technique to provide information about local magnetic properties, correlation between the particle moments, and the internal field distribution [7–10]. The magnetic resonance study of assemblies of nanoparticles is interesting because the magnetic properties of the surface atoms differ radically from the corresponding bulk atoms. It is also known that surface spins resist from being aligned with even a large external magnetic field [11], which gave rise to the conception of spin canting [12]. As it is well known, the magnetic response of the nanoparticle system to the external field depends on the cation distribution [13], temperature, and size [14]. On Mn_{1-x} Zn_x Fe_2O_4, Rath et al. [14] found a change in the crystallite size between 4.5 nm and 10.5 nm in the $0 < x < 1$ range for nanoparticles prepared via hydrothermal precipitation method. Arulmurugan et al. [15] found similar values for nanoparticles prepared by chemical precipitation method. In this paper, the EPR and VSM techniques are used to study the magnetic properties of magnetic nanoparticles synthesized by normal micelle micro-emulsion method at room temperature.

2. Experiment

Magnetic nanoparticles were synthesized by normal micelle micro-emulsion method at room temperature [16, 17]. Sodium dodecylsulfate was used as the surfactant, added to an aqueous solution containing soluble

$FeSO_4$, $ZnSO_4$, and $MnSO_4$; hence, the normal micelles are formed. A 6 M NaOH solution is added to the previous solution, which shows a dark appearance. It is, then, stirred for 2 h. The spinel structure is formed when H_2O_2 (30%) is added by the complete oxidation of Fe^{2+} to Fe^{3+}. The ratio between Mn/Zn and Fe cations is adjusted to 1:2 for every sample, the value of x varied in the $0 < x < 0.75$ range (see Table II).

TABLE II

Nanoparticles size for different x concentration

Sample	Nanocrystallite size D [nm] from the Scherrer formula	Nanoparticle size D [nm] from AFM images
$X = 0$	39	49 ± 4
$X = 0.25$	31	32 ± 4
$X = 0.5$	26	28 ± 6
$X = 0.75$	15	17 ± 3

The size measurements were performed on an Asylum Research MFP-3D AFM. The height channel was corrected using the sensor in the Z-direction that this instrument features (closed loop in the three axis) by performing line-by-line (of scanning) fits between the two signals (Z-sensor and height). Repeated measurements were carried to ensure that the particles were mono-dispersed and well attached on the mica surface. Measured diameters were calculated from height histograms on masked images (considering only the apex of the particles). The magnetic behavior was studied by EPR technique by using a Bruker EPR-300 spectrometer in the X-band frequency range, at 170–350 K. The magnetization curves were measured by using vibrating spectro-magnetometer (VSM) from Quantum Design^{TM} physical property measuring system (PPMS).

3. Results

The ferrite structure was identified by XRD, where peaks can be indexed to planes (220), (311), (400), (422), (511), and (440) of single-phase MnZn ferrite (see Fig. 1). From the Scherrer equation:

$$B = \frac{k\lambda}{L\cos\theta}, \tag{1}$$

we obtained experimental nanocrystallite size values from 39 nm to 15 nm for $x = 0$ and $x = 0.75$ respectively, as presented in Table II. In Eq. (1) B is the width of the diffraction peak after subtracting the instrumental effect, λ the wavelength of the x-ray used, $k \approx 1$ for cubic crystals and θ is the Bragg angle. As is expected [15], the particle size decreases with the increase in the Zn concentration. These values correspond to the magnitude expected by Rondinone's approach [17]. This last method correlates nanoparticle size to synthesis conditions: metal salt concentration, sodium hydroxide concentration, and temperature. Using Rondinone's approach, the mean value for nanoparticle size was estimated roughly as $D = 33.1 \pm 0.1$nm.

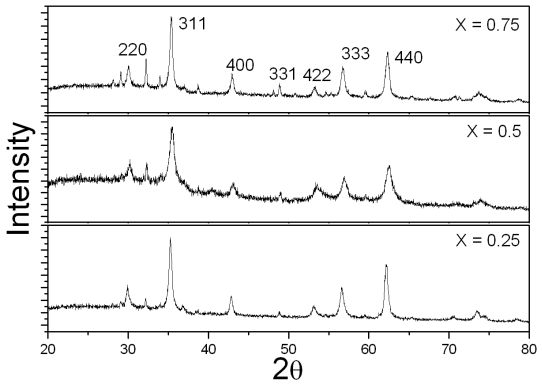

Fig. 1. DRX of $Mn_xZn_{1-x}Fe_2O_4$.

AFM measurements have been carried out on $Mn_{1-x}Zn_xFe_2O_4$ ferromagnetic nanoparticle samples deposited on mica substrates (see Fig. 2). Sample preparation required dispersing the particles on the surface of the mica by diluting them (typical concentration 0.5×10^{-9} g in 10×10^{-6} l) and dispersing them (through sonication), then placing a drop on top of the fresh cleaved mica and letting it dry.

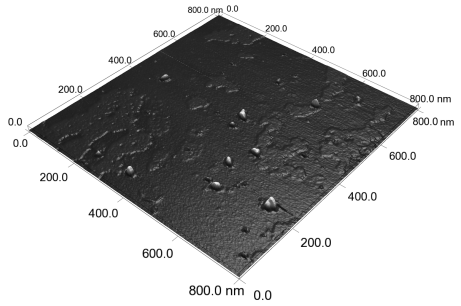

Fig. 2. AFM image of $ZnFe_2O_4$ nanoparticles.

4. Magnetic properties

For $x > 0.5$, the EPR spectra consist of a single resonance signal, strongly symmetrical, with $g \approx 3.25$ (see Fig. 3a) and a resonant field approximately constant $H_r \approx 2073$ G. This signal is attributed to the ions Fe^{3+} distributed in octahedral coordinates sites. While the x concentration decreases, the symmetry of the signal reduces (see Fig. 3b and 3c), indicating a random distribution of the anisotropy in the system, with perpendicular and parallel modes, giving information about the effective anisotropy of the system.

For each concentrations x, the central field remains approximately constant as a function of the temperature (see Fig. 4).

The peak to peak line width ΔH_{PP} at 180 K presents a maximal value for $x = 0.25$ (see Table III). Above $x > 0.25$, ΔH_{PP} decreases when x increases (shown in Fig. 4).

TABLE III

Peak to peak line width ΔH_{PP} from EPR spectrum

Sample	Temperature [K]	Peak to peak line width ΔH_{PP} [G] ±3%
$x = 0$	180	940
$x = 0.25$	180	1038
$x = 0.50$	180	717
	210	605
	250	470
$x = 0.75$	180	650

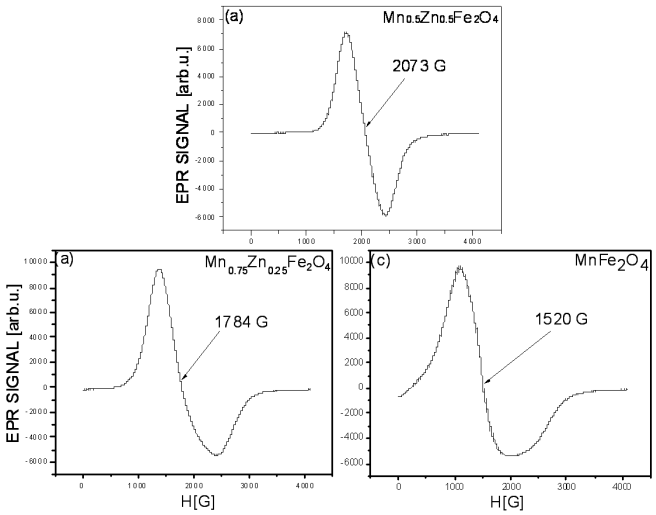

Fig. 3. EPR signal at T=180 K, (a) x=0.0, (b) x=0.25 and (c) x=0.50.

It is interpreted as a reduction of the effect of magnetic interaction (local fields), due to a reduction of magnetic ions (i.e. Mn ions) per unit cell. This behavior is similar to the behavior predicted by the model for solid solutions with magnetic dilution (1-x): $\Delta H_{PP} \propto (1-x)^{1/2}$. The behavior $0 < x < 0.25$ indicates the existence of a critical grain size for the transition from single to multi-domain regime for nanoparticles which size increases from 32 nm to 49 nm with the subsequent reduction in ΔH_{PP}.

The effect of the temperature can be observed on the sample $x = 0.5$ (indicates in Fig. 5), where ΔH_{PP} shows

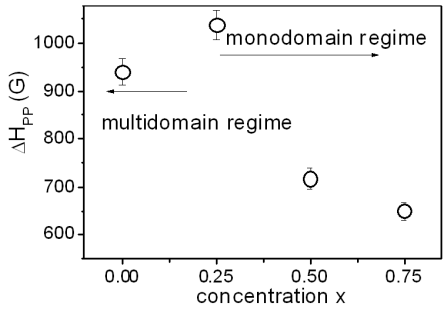

Fig. 4. EPR signal for different concentrations of $Mn_{1-x}Zn_xFe_2O_4$ at 180K.

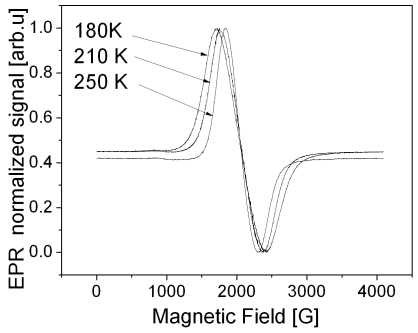

Fig. 5. EPR normalized signals for $x = 0.50$.

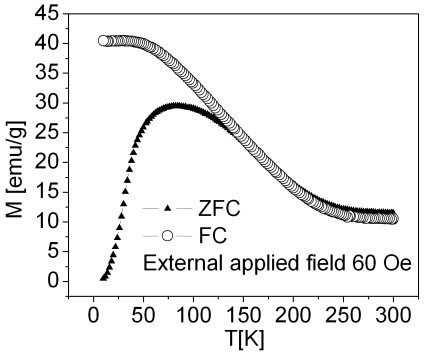

Fig. 6. Temperature-dependence of the magnetization under zero field-cooling (ZFC) and field-cooling (FC) for $x = 0.75$.

a marked increase with decreasing temperature, e.g. the growth up of magnetic domains with strong ferromagnetic correlated spins.

Fig. 6 shows the zero-field cooling (ZFC) and field-cooling (FC) magnetization curves measured for $x = 0.75$ at 60 Oe corresponding to a typical assembly of small magnetic particles. The ZFC curve shows a broad maximum located at 82 K which originated from freezing processes due to interparticle interactions. The FC is very flat below 40 K in comparison with the monotonously increasing behavior characteristic of noninteracting systems [18, 19]. This behavior reinforced the existence of strong interactions among particles.

5. Conclusions

EPR and magnetization measurements of $Mn_xZn_{1-x}Fe_2O_4$ nanoparticles synthesized by a normal micellar technique are reported. The concentration was varied in the $0 < x < 0.75$ range. For $x > 0.5$, a single resonance signal, strongly symmetrical is observed. This line is attributed to the ions Fe^{3+} distributed in octahedral coordinates sites. For low x concentration the symmetry of the signal EPR reduces indicating a random distribution of the anisotropy in the system, with perpendicular and parallel modes, giving information about the effective anisotropy of the system.

From the ΔH_{PP} behavior we suggest the existence of a critical monodomain size between 32 nm to 49 nm. The flattening of the MFC evidences the presence of strong interparticle interactions at low temperatures.

Acknowledgements

This work was partially supported by the "Patrimonio Autónomo Fondo Nacional de Financiamiento para la Ciencia, la Tecnología y la Innovación Francisco José de Caldas" No 275–2011.

References

[1] G. Ott, J. Wrba, R. Lucke, *J. Magn. Magn. Mater.*, **254–255**, 535, (2003).

[2] Q.A. Pankhrust, J. Connolly, S.K. Jones, J. Dobson, *J. Phys. D*, **36**, 167, (2003).

[3] U. Häfeli, W. Schütt, J. Teller, M. Zborowski, *Editors, Scientific and Clinical Application of Magnetic Carriers*, Plenum Press, New York, (1997).

[4] A.H. Morrish, P.E. Clark, *Phys. Rev. B*, **11**, 282, (1975).

[5] R. Justin Joseyphus, A. Narayanasamy, K. Shinoda, B. Jeyadevan, K. Tohji, *J. Phys. Chem. Solids*, **67**, 1510 (2006).

[6] J. Wang, C. Zeng, Z. Peng, Q. Chen, *Physica B*, **349**, 124, (2004).

[7] J.P. Jamet, A.P. Malozemoff, *Phys. Rev. B*, **18**, 75, (1978).

[8] F. Gazeau, J. C. Bacri, F. Gendron, R. Perzynski, Yu. L. Raikher, V. I. Stepanov and F. Dubois, J. Magn. Mater. **186**, 175, (1998).

[9] E. De Biasi, C.A. Ramos, R.D. Zysler, H. Romero, *Phys. Rev. B*, **65**, 144416, (2002).

[10] R. Berger, J. Kliava, J.C. Claude Bissey, *J. Appl. Phys.*, **87**, 7379, (2000).

[11] A.E. Berkowitz, W.J. Shuele, P.J. Flanders, *J. Appl. Phys.*, **39**, 1261, (1968).

[12] J.M.D. Coey, *Phys. Rev. Lett.*, **27**, 1140, (1971).

[13] D.J. Fatemi, V.G. Harris, M.X. Chen, S.K. Malik, W.B. Yelon, G.J. Long, A. Mohan, *J. Appl. Phys.*, **85**, 5172, (1999).

[14] C. Rath, S. Anand, R.P. Das, K.K. Sahu, S.D. Kulkarni, S.K. Date, N.C. Mishra, *J. Appl. Phys.*, **91**, 2211, (2002).

[15] R. Arulmurugan, B. Jeyadevan, G. Vaidyanathan, S. Sendhilnathan, *J. Magn. Magn. Mater.*, **288**, 470, (2005).

[16] A.J. Rondinone, A.C.S. Samia, Z.J. Zhang, *J. Phys. Chem. B*, **103**, 6876, (1999).

[17] A.J. Rondinone, A.C.S. Samia, Z.J. Zhang, *J. Phys. Chem. B*, **104**, 7919, (2000).

[18] G.A. Mendoza, O. Guzmán, H. Ariza-Calderón, P. Prieto, *J. Appl. Phys.*, **97**, 10A507, (2005).

[19] E. De Biasi, C.A. Ramos, R.D. Zysler, *Phys. Rev. B* **65**, 144416, (2002).